Chinese Journal of
POLYMER SCIENCE

RESEARCH ARTICLE

https://doi.org/10.1007/s10118-022-2760-y
Chinese J. Polym. Sci. **2023**, *41*, 14–23

Improvement on the Mechanical Performance and Resistance Towards Hydrolysis of Poly(glycolic acid) *via* Solid-state Drawing

Jia-Xuan Li[a], De-Yu Niu[a], Bo Liu[a], Peng-Wu Xu[a], Wei-Jun Yang[a], Pieter Jan Lemstra[a,b], and Pi-Ming Ma[a*]

[a] *The Key Laboratory of Synthetic and Biological Colloids, Ministry of Education, Jiangnan University, Wuxi 214122, China*
[b] *PlemPolco B.V., Roek 24, 5508 KE Veldhoven, the Netherlands*

Electronic Supplementary Information

Abstract Poly(glycolic acid) is a biocompatible as well as biocomposable polymer with superior mechanical and barrier properties and, consequently, has found important applications in both medical and packaging fields. However, the high hydrolysis rate in a high humidity environment restricts its application. In this work, a solid-state drawing process after melt extrusion is applied in order to produce fibrous PGA with enhanced mechanical properties and a much better resistance towards hydrolysis. The crystal structure of PGA gradually transformed from spherulites into oriented fibrous crystals in the stretching direction upon solid-state drawing. Meanwhile, both the length of microfibril and the size of lamellae increased initially with the drawing ratio (DR), while the chain-folded lamellae transformed into extended-chain fibrils at high(er) DR. The oriented structures lead to an overall improvement of the mechanical properties of PGA, *e.g.*, the tensile strength increased from 62.0±1.4 MPa to 910±54 MPa and the elongation at break increased from around 7% to 50%. Meanwhile, the heat capacity of totally mobile amorphous PGA (ΔC_p^0=0.64 J·g^{-1}·°C^{-1}) was reported for the first time, which was used to analyze the content of mobile amorphous fraction (X_{MAF}) and rigid amorphous fraction (X_{RAF}). Both the oriented chain-folded lamellae crystals and the tightly arranged RAF are beneficial to prevent water molecules from penetrating the matrix, thus improving the resistance towards hydrolysis. As a consequence, the fibrous PGA with a DR of 5 showed a tensile strength retention rate of 17.3% higher in comparison with the undrawn sample after 7-days accelerated hydrolysis. Therefore, this work provides a feasible method to improve the mechanical and resistance towards hydrolysis performance of PGA, which may broaden its application and prolong the shelf-life of PGA products.

Keywords Poly(glycolic acid); Solid-state drawing; Fibrous crystal; Mechanical property; Hydrolysis resistance

Citation: Li, J. X.; Niu, D. Y.; Liu, B.; Xu, P. W.; Yang, W. J.; Lemstra, P. J.; Ma, P. M. Improvement on the mechanical performance and resistance towards hydrolysis of poly(glycolic acid) *via* solid-state drawing. *Chinese J. Polym. Sci.* **2023**, *41*, 14–23.

INTRODUCTION

The biodegradable polymer, poly(glycolic acid) (PGA) has the simplest chemical structure in the linear polyester family, and possesses many advantageous properties, such as a high mechanical strength and gas barrier property.[1] The unit cell of PGA belongs to orthorhombic system (*a*=5.22 Å, *b*=6.19 Å, *c*=7.02 Å),[2] and two PGA molecular chains in plane zig-zag conformation are arranged in a unit cell, where each chain has two glycolic acid units. It was found that the C(O)—O bond length of PGA is smaller and O—C(O)—CH_2 bond angle is larger than those of other polyesters, indicating that the molecular chain and the ester groups could arrange much closer in the lattice. As a consequence, PGA exhibits excellent mechanical properties and gas barrier properties, also high(er) melting point (~230 °C), but the drawback is a high density (~1.58 g·cm^{-3}). These characteristics have enabled PGA to be favored in applications such as oil extraction fracturing plugs and barrier packaging materials.[3]

The most important application of PGA is in the biomedical field due to its excellent biocompatibility and biodegradability, and PGA is actually the first biodegradable man-made polymer used in the biomedical industry.[1] However, the application of PGA serving as packaging materials has become more and more popular since large-scale production of PGA with low(er) cost was commercialized by Kureha company in USA and Pujing company in China. For medical application, a long(er) shelf-life of, *e.g.*, suture, is needed. However, the degradation of PGA due to hydrolysis is too fast to guarantee the quality of commercial products even during storage. For example, the M_n of PGA decreased from 3×10^4 to 5×10^3 after three days in a buffer solution at 37 °C, and the mass loss about 60% after 24 days.[4] Therefore, improving the shelf-life of PGA, *e.g.*, the hydrolysis resistance, is of importance to broaden its application.

To improve the hydrolysis resistance of polymeric materi-

* Corresponding author, E-mail: p.ma@jiangnan.edu.cn

Invited Research Article for Special Issue "Ordered Structure of Polymers".
Received March 18, 2022; Accepted April 18, 2022; Published online July 20, 2022

als, many methods have been reported. One simple method is to directly incorporate the hydrolytic stabilizers, such as carbodiimides and oxazolines,[5,6] or non-hydrolysis components to improve the structural stability and hydrolysis behavior.[7] Besides, adjusting the chemical structure composition can also enhance the hydrolysis resistance.[8,9] For example, it was found that the hydrolysis resistance of poly(lactic-*co*-glycolic acid) (PLGA) could be improved due to the regulation of the composition and structure.[10] Similar methods such as incorporating the hydrophobic segments into the polymer chains[11] or designing hydrophobic surfaces were also reported.[12]

Usually, the hydrolytic stabilizer increases the cost price and therefore, it will be interesting to improve the stability of polymeric materials by adjusting only the processing technology or performing pre/post treatment where the physical structures, *e.g.*, crystalline and amorphous structure can be well tuned.[13–15] Recently, it has been reported that the crystalline structure of PGA suture was adjusted by annealing under axial stress leading to thicker and ordered lamellae.[16] Consequently, the strength of the PGA suture was increased, and the ingress of water molecules was hindered by regulated crystalline structures resulting in better hydrolysis stability. Besides crystalline structure, the amorphous region notably the rigid amorphous fraction (RAF) would also affect the properties of materials.[17,18] RAF is an oriented amorphous region with higher stiffness and T_g in comparison with completely mobile amorphous fraction (MAF). Such RAF has been identified by using solid-state ^{1}H-NMR spectroscopy in highly stretched PGA. After stretching, the PGA crystals show an anisotropy mechanical property due to the orientation of polymer chains in the stretching direction (SD). The crystal modulus in the stretching direction was reported to be as high as 300 GPa, while the longitudinal shear modulus was only 6 GPa.[19,20] Interestingly, it was found that the formation of RAF in PLA films after biaxially stretching could obviously hinder water molecular diffusion,[21] indicating that it might be a new way to improve the hydrolysis resistance of PGA by controlling the RAF formation and the crystalline morphology.

Herein, a versatile solid-state drawing route after melt extrusion was adopted in this work, aiming to make fibrous PGA with high tensile strength and hydrolysis resistance by tailoring the crystalline and amorphous structures simultaneously. Moreover, the evolution in the condensed and orientated structure in both amorphous and crystalline regions during the solid-state drawing was studied, and its effect on the hydrolysis of fibrous PGA was correlated. Therefore, this work provides a simple method to achieve superior tensile strength and hydrolysis resistance of PGA materials, which may enable a longer shelf-life of PGA commodity products and broaden their application range.

EXPERIMENTAL

Materials

PGA (M_n=1.5 × 10^5 g/mol and M_w/M_n=1.3) in the form of pellets was supplied by Shanghai Pujing Chemical Industry Co., Ltd., China. The solvent hexafluoroisopropanol (HFIP) (Sigma-Aldrich) were used as received.

Sample Preparation

PGA pellets were dried at 80 °C under vacuum oven for 12 h before use. Haake extruder (Rheomex PTW, Germany) was used for fibrous PGA preparation. The temperature control of the extruder was set around 230 °C and the screw speed was set as 50 r/min. The extrudates were quenched by using cold water bath and further drawn at an elevated temperature (around 50 °C) in air to make thin fibrous PGA up to 100 μm. The sample with a drawing ratio (DR) of x is marked as DR-x and the extrudate without drawing was marked as DR-0.

Characterization

Small /wide angle X-ray scattering (SAXS, WAXS)

SAXS and WAXS tests on fibrous PGA were conducted on XEUSS 3.0 system, France, equipped with a Copper internal source (Genix3D) that produced an X-ray beam (λ=0.15418 nm) with energy of 8 keV. The sample to detector distance in the SAXS test was 1800 mm, and 60 mm for WAXS test. High resolution mode was selected, the spot size was 0.8 mm × 0.5 mm. The exposure time was 600 s for both the SAXS and WAXS tests. LaB_6 was used to calibrate the distance before experiment. The data were processed with XSACT and Foxtrot software, and the effects of background scattering, air scattering and light fluctuations were deducted in advance. In 2D WAXS and SAXS patterns, the horizontal direction is the stretching direction.

Long period: The electron density correlation function $K(z)$ was applied to obtain the long period in meridian direction (L_m), amorphous thickness (L_a) and crystalline thickness (L_c) by the inverse Fourier transformation given as follows:

$$K(z) = \frac{\int_0^\infty I(q)\, q^2 \cos(qz)\, \mathrm{d}q}{\int_0^\infty I(q)\, q^2 \mathrm{d}q} \quad (1)$$

where z is the axis parallel to the stretching direction, and $I(q)$ is the intensity of 1D SAXS profile. The smaller value was assigned as the average L_c, and the L_a can be calculated by $L_a = L_m - L_c$.

Orientation parameter (f): The orientation parameter of PGA with different DRs was estimated from the value of Herman's orientation function:[15]

$$f = \frac{3\left(\cos^2\varphi\right)_{hkl} - 1}{2} \quad (2)$$

$\cos^2\varphi$ is an orientation factor defined as Eq. (3):

$$\cos^2\varphi = \frac{\int_0^{\pi/2} I(\varphi) \cos^2\varphi \sin\varphi \mathrm{d}\varphi}{\int_0^{\pi/2} I(\varphi) \sin\varphi \mathrm{d}\varphi} \quad (3)$$

where φ is the azimuthal angle and $I(\varphi)$ is the scattered intensity along azimuthal angle. $I(\varphi)$ was analyzed at the (110) reflection of PGA.

Mechanical properties

Mechanical properties of fibrous PGA were measured at ambient temperature using a universal tester (Instron 5967, USA) according to G/BT 529-2008 at a crosshead speed of 50 mm/min. Five specimens of each sample were examined and the averaged values were presented.

Accelerated hydrolysis aging test

The accelerated hydrolysis aging test on fibrous PGA was conducted in 40 °C and 80% humidity. The aged samples were taken out at an interval of 1, 3, 5, and 7 days, respectively, and dried for 1 week using a freeze dryer to remove the residual

https://doi.org/10.1007/s10118-022-2760-y

moisture for the subsequent characterization.

Temperature-modulated differential scanning calorimetry (TMDSC)

DSC (NETZSCH 204 F1, Germany) was used for both standard DSC and TMDSC analysis. Around 5 mg of each sample was heated from 0 °C to 260 °C at 10 °C/min under nitrogen atmosphere. In particular, for the analysis of melting point and crystallinity of the aged samples, the above thermal procedure was followed by cooling down to 0 °C and reheating to 260 °C at 10 °C/min. For TMDSC tests, a heating rate of 3 °C/min, an oscillation period of 60 s and a temperature modulation amplitude of ±0.5 °C were applied. The calculation procedures of crystallinity (X_c), the content of mobile amorphous fraction (X_{MAF}), and the content of rigid amorphous fraction (X_{RAF}) are shown in Eqs. (4)–(6):

$$X_c = \Delta H_m / \Delta H_m^0 \times 100\% \quad (4)$$

$$X_{MAF} = \Delta C_p / \Delta C_p^0 \quad (5)$$

$$1 = X_c + X_{MAF} + X_{RAF} \quad (6)$$

where ΔH_m is the enthalpy of melting of the sample, and ΔH_m^0 is the enthalpy of melting for 100% crystalline PGA (135.0 J/g).[22] ΔC_p is the reversible heat capacity increase in glass region. ΔC_p^0 is the heat capacity for totally mobile amorphous PGA, which is calculated as 0.64 $J \cdot g^{-1} \cdot °C^{-1}$, and is the first time reported in this work.

Fourier transform infrared spectroscopy (FTIR)

The chemical structure of accelerated aged PGA samples was identified by FTIR (Nicolet 6700, Thermo Fisher Scientific, USA) with an attenuated total reflection (ATR) mold. 32 scans were performed for each sample at a resolution of 4 cm^{-1} over a range of 500–4000 cm^{-1}.

Intrinsic viscosity measurement

The PGA/HFIP solutions of accelerated aged samples were prepared with a concentration of 0.1 g/dL, and the intrinsic viscosity of the samples was measured in Ubbelohde viscometer at 25 °C using the one-point method according to Eqs. (7) and (8):

$$[\eta] = \left[2\left(\eta_{sp} - \ln\eta_r\right)\right]^{1/2} / C \quad (7)$$

$$\eta_{sp} = \eta_r - 1 \quad (8)$$

where η_r is the relative viscosity, which is calculated from the ratio of the outflow time t of the PGA/HFIP solution and the outflow time t_0 of the pure solvent. η_{sp} is the specific viscosity, and C is the concentration of the PGA/HFIP solution.

RESULTS AND DISCUSSION

Effect of Solid-state Drawing on the Mechanical Properties of Fibrous PGA

The stress-strain curves and corresponding tensile strength of solid-state drawing fibrous PGA with different drawing ratios (DRs) are shown in Fig. 1. The tensile strength of DR-0 is only 62.0±1.4 MPa. However, after solid-state drawing, the tensile strength is significantly increased to 340±30, 420±30 and 910±54 MPa for DR-3, DR-5 and DR-7, respectively, *i.e.*, the tensile strength was increased by around 1400% after drawn 7 times. Meanwhile, solid-state drawing fibrous PGA possesses superior tensile toughness with an elongation at break of 20%–50% in comparison with DR-0 of below 10%. The effect of solid-state drawing on the tensile strength of fibrous PGA is related to the evolution of the amorphous and crystalline structure, and it will be discussed in The Evolution of Crystalline Structure of Fibrous PGA upon Solid-state Drawing.

The Evolution of Crystalline Structure of Fibrous PGA upon Solid-state Drawing

In order to monitor the evolution of the crystalline structure of PGA upon solid-state drawing, WAXS and SAXS were applied to characterize fibrous PGA with different DRs. The 2D WAXS patterns are shown in Fig. 2(a), and the stretching direction has been marked with a black arrow.

Two obvious scattering rings are observed in the 2D WAXS pattern of DR-0, which are correspond to the scattering peaks of (110) crystal plane (2θ=22.2°) and (020) crystal plane (2θ=28.7°) of PGA,[1] respectively. The intensity distribution of DR-0 is uniform in the azimuth range of 0°–360°. As the DR increases, the PGA crystals becomes better orientated. Firstly, the scattering rings of fibrous PGA become diffuse with the DR increasing from 0 to 3, and then obvious scattering arcs appear in the WAXS pattern of DR-5 with the intensity focus towards equator. When the drawing ratio increases to 7, the scattering arcs transform to concentrated points, indicating that the PGA crystals have highly orientated in the stretching direction.

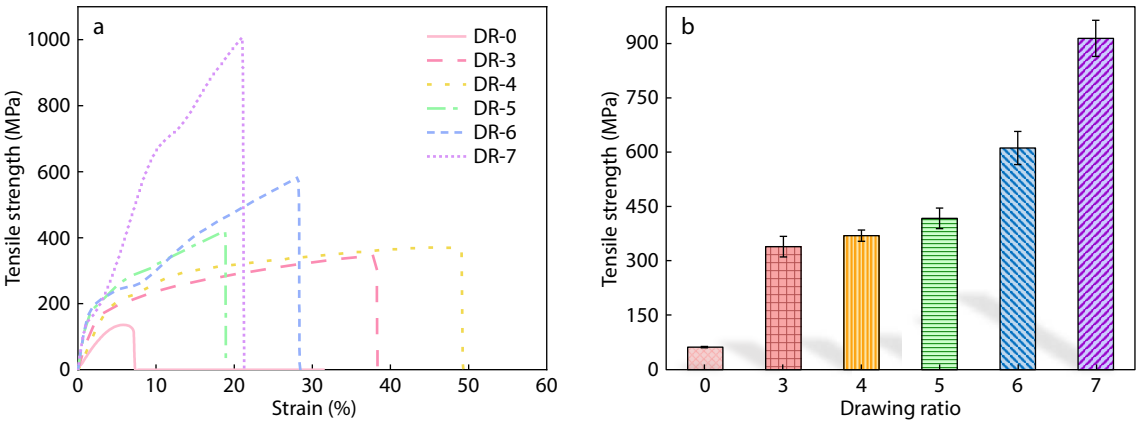

Fig. 1 (a) Stress-strain curves and (b) tensile strength of fibrous PGA with different DRs.

https://doi.org/10.1007/s10118-022-2760-y

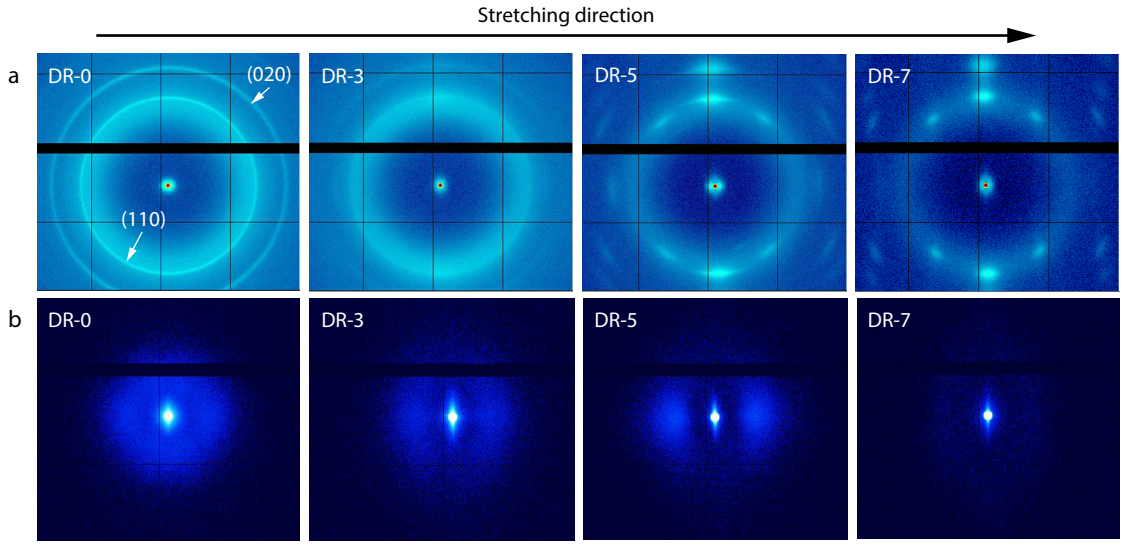

Fig. 2 2D WAXS (a) and SAXS (b) patterns of fibrous PGA with different DRs.

Fig. 2(b) shows the 2D SAXS patterns of fibrous PGA with different DRs (more patterns are available in Fig. S1 in the electronic supplementary information, ESI). The SAXS pattern of the DR-0 sample is elliptic iso-intensity contour shaped due to the initial non-oriented spherulites. As the DR increases, the orientation of the lamellae in the stretching direction became obvious, and microfibril structure was formed at the DR of 3, as indicated by the streak signal in the equator.[23] Interestingly, two obvious lobule-shaped scattering signals in the case of DR-5 appear on both sides of the beam stop over a large azimuthal angle range, confirming the formation of oriented chain-folded lamellar structure (*i.e.*, kebab crystals). Subsequently, the lobule-shaped signal attributes to the chain-folded lamellae disappears and only the sharp streak signal in the equator can be seen when the DR further increases to 7, which is probably due to the scattering of extended-chain fibrils.

To summarize, the crystals of fibrous PGA gradually changed from non-oriented spherulites to fibrous crystals structure (or the term "shish-kebab" used in other studies) with increasing the DR up to a mediate value of such as 5, while the lamellae crystals could transform into extended-chain fibrils at higher DRs.

1D WAXS azimuthal integrated intensity curves of (110) plane are illustrated in Fig. 3(a), showing two crystal plane peaks of the fibrous PGA located at 90° and 270°. As DR increases, the peaks became narrower and sharper, indicating a stronger orientation of PGA crystals along the stretching direction. The orientation parameter (f) can be calculated by fitting the azimuthal integral intensity distribution curve of the 2D WAXS pattern *via* Eqs. (2) and (3). The changes of f with DR are shown in Fig. 3(b). Apparently, DR-0 has almost no orientation structure (f=0.09), while the f significantly increases up to 0.646 as the DR increases to 7. By solid-state drawing, the crystals are oriented in the stretching direction, compared with the crystals with low orientation, the tensile strength of fibrous PGA can be highly improved.

In order to obtain the periodic information of the lamellae arrangement in the stretching direction, the 1D scattering intensity distribution curves were obtained by integrating the 2D SAXS patterns and Lorentz corrected, as shown in Fig. 3(c). Long period in the meridian direction (L_m), amorphous thickness (L_a) and crystalline thickness (L_c) were calculated by Eq. (1), the method and results are shown in Fig. 3(c).

When the DR is larger than 3, the L_m decreases with increasing the DR. This phenomenon refers to a slipping of lamellae stacks during stretching accompanied by lamellae bending, which may cause the reduction of long period and the formation of microfibril structure in the stretching direction.[24] Further increasing DR from 3 to 5, the lamellae crystals grow on the microfibril leading to an increase in L_c, which is consist with the variation of the 2D SAXS patterns. With the further increase of DR, strain-induced fragmentation-recrystallization may happen in the chain-folded lamellae,[25] and gradually break and rearrange into extended-chain fibrils at a high(er) drawing ratio, which leads to a decrease in L_c. Fragmentation-recrystallization is a process in which the folded chains of lamellae break and rearrange under tensile stress, also known "local melt-recrystallization". The stretching above T_g reduce the nucleation barrier *via* formation of locally ordered structures and consequently induces secondary crystallization, thus the L_m and L_a decreases as well with the DRs.[26] That is, the structural evolution of the original non-oriented crystals was accompanied by the generation of new crystals during the solid-state drawing process.

The intensity and dimension changes of chain-folded lamellae and microfibril structure during solid-state drawing were calculated to further study the strain-induced lamellae structure transformation. Firstly, the relative scattering intensity of the lamellae crystal ($I_{lamellae}$) and the lateral size of lamellae ($L_{lateral}$) are calculated by using an integration method (Fig. S3 in ESI), as shown in Fig. 4(a) and Fig. 4(b), respectively. The $I_{lamellae}$ increases with DR up to 5, and then decreases dramatically. At the early stage, the isotropic PGA lamellae stacks undergo slipping up on stretching, resulting in lamellae crystals with a certain extent of orientation. The lamellae crystals grow subsequently with further increasing the DR as evidenced by the increase of both $I_{lamellae}$ and $L_{lateral}$

https://doi.org/10.1007/s10118-022-2760-y

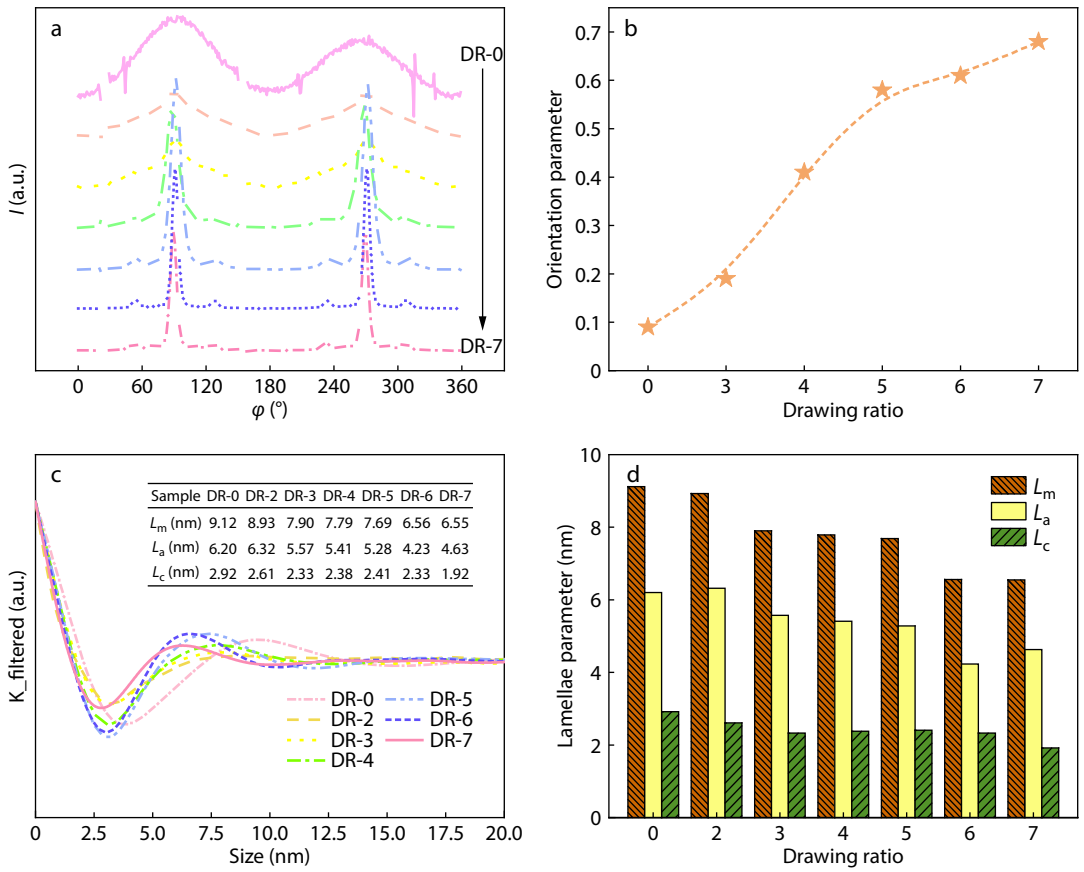

Fig. 3 (a) Azimuthal integral intensity distribution curves of the 2D WAXS patterns, (b) orientation parameter (*f*), (c) the analysis of lamellae structure using correlation function, (d) long period (L_m), amorphous thickness (L_a) and crystalline thickness (L_c) for fibrous PGA with different DRs.

due to the better folding of PGA chains in the stretching direction. However, the chain-folded lamellae gradually transform into extended-chain microfibrils as confirmed by a drop in both $I_{lamellae}$ and $L_{lateral}$ at high DRs (*e.g.*, DR=6–7), due to the fragmentation-recrystallization in lamellae stacks and the disentanglement of polymer chains.

The length of the microfibril (L_{MF}) in the fibrous PGA is obtained by Ruland's method.[27–29] Different q values were chosen to scan the scattering intensity in the azimuthal angle range of 0° to 180°, and the half-height width of the corresponding curves is marked as B_{obs}. The relationship between B_{obs}, L_{MF}, and the misorientation of microfibril (B_φ) can be described by Eq. (9):

$$B_{obs} = \frac{2}{\langle L_{MF} \rangle q} + B_\varphi \quad (9)$$

On the basis of Eq. (9), L_{MF} can be obtained from the slope of the fitted line between B_{obs} and q^{-1}. The specific fitting process is shown in Fig. 4(d). The change of the L_{MF} with DRs is shown in Fig. 4(c). Short microfibrils with an average length of ~38 nm firstly appears at the DR of 3. While the L_{MF} increases continuously with increasing the DR, and reaches around 213 nm with the DR up to 7. Apparently, the chain-folded lamellae gradually transform into longer and extended microfibril structures at high(er) drawing ratios, which is also consistent with the above discussion on crystal structure evolution.

MAF to RAF Transition in Amorphous Region of Fibrous PGA upon Solid-state Drawing

The effect of solid-state drawing on the amorphous region of PGA was further studied combining with a three-phase model of polymer crystallization.[30] TMDSC test was also carried out on the samples with various DRs, and the results are shown in Fig. 5(a). The heat capacity of fibrous PGA in the glass transition region gradually decreases with the increase of DRs, but the T_g increases. The calculation method of both the content of mobile amorphous fraction (X_{MAF}) and rigid amorphous fraction (X_{RAF}) has been described in the experimental section, Eqs. (4)–(6), and the results are shown in Fig. 5(b). Since the standard heat capacity for completely mobile amorphous PGA (ΔC_p^0) is not known yet, it is calculated and reported here as 0.64 J·g^{-1}·°C^{-1} for the first time according to the Czerniecka-Kubicka method,[31] also see detailed calculation in Fig. S2 in ESI. The intersection of the fitted line and X axis (*i.e.*, 135.4 J·g^{-1}) is called enthalpy of fusion for fully crystalline of PGA, which is close to the reported value (*i.e.*, 135.0 J·g^{-1}) in literature by Nishino.[22]

Solid-state drawing above T_g can promote the molecular chain orientation and reduce nucleation barrier, therefore, the crystallinity X_c of fibrous PGA gradually increases as the DR increases. As a result, the mobile amorphous fraction (MAF) was consumed heavily and the X_{MAF} decreases rapidly. Meanwhile, the content of rigid amorphous region (X_{RAF}) increases during stretching. The RAF is an oriented amorphous

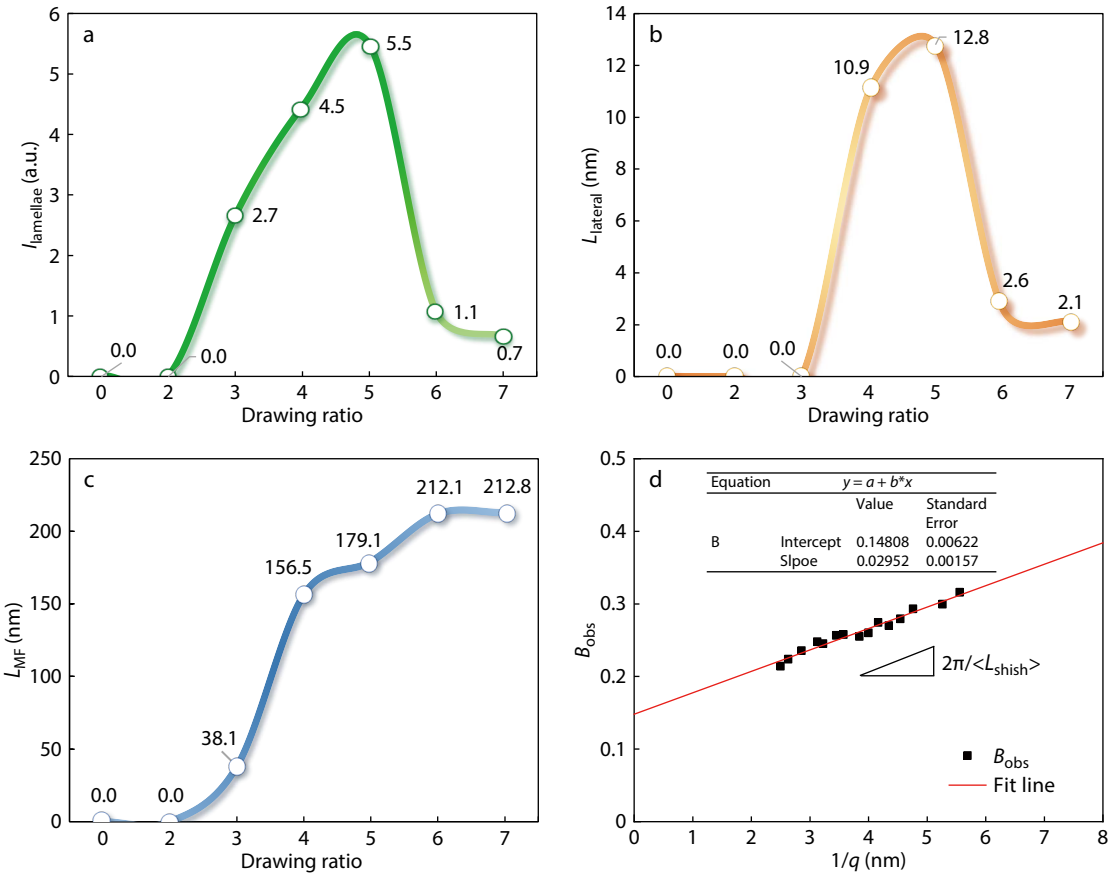

Fig. 4 (a) Relative scattering intensity of chain-folded lamellae structure, (b) the lateral size of lamellae structure ($L_{lateral}$), (c) average microfibril length (L_{MF}) of fibrous PGA with different DRs, (d) linear plot of azimuthal integral width (B_{obs}) versus 1/q, which is used to calculate the L_{MF}.

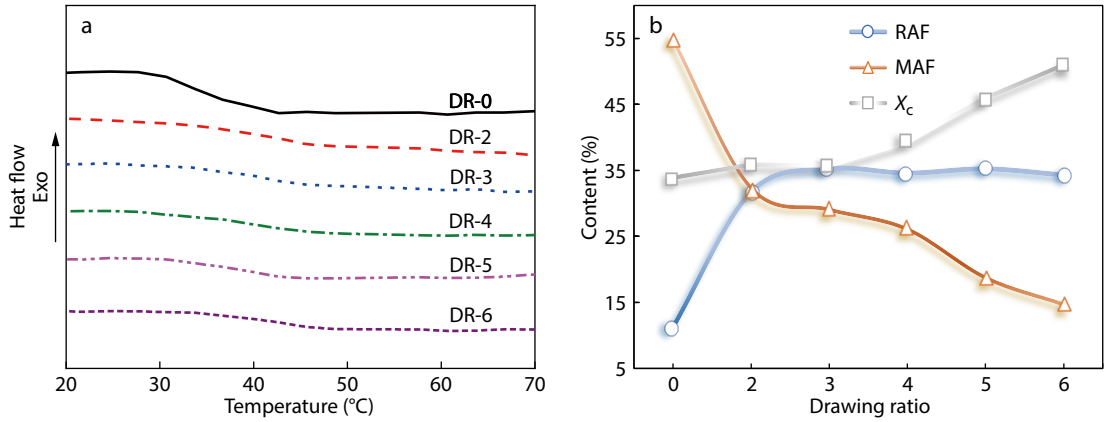

Fig. 5 (a) TMDSC reversible heat flow curves, (b) the content of mobile amorphous fraction (X_{MAF}), rigid amorphous fraction (X_{RAF}) and crystallinity (X_c) of samples with different DRs. The DSC heating curves of samples with different DRs are shown in Fig. S4 (in ESI), which are used to calculate X_c.

region between the crystalline region and the mobile amorphous region, having higher stiffness in comparison with MAF. The X_{RAF} increases with DR and tends to stabilize after the DR reaches 3, as shown in Fig. 5(b). It is known that, a hydrolysis of polyesters usually starts from the amorphous region and is closely related to free volume which affects the diffusion of water molecules,[32,33] *i.e.*, the larger free volume the easier for water molecules to penetrate into the matrix to break the ester bonds. Since both RAF and crystalline regions are arranged tightly with smaller free volumes in comparison with MAF, the increase in X_{RAF} and crystallinity would increase the resistance of PGA to hydrolysis.

Effect of Solid-state Drawing on Hydrolysis Behavior of Fibrous PGA

Based on the above discussion on structure evolution, the sample DR-5 with the strongest $I_{lamellae}$ and the largest lateral

https://doi.org/10.1007/s10118-022-2760-y

size was selected for accelerated aging experiment (40 °C, 80% humidity) with the DR-0 as a control sample. The mechanical properties of the samples are recorded as a function of accelerated aging time, as shown in Fig. 6. The variation trends of tensile strength are almost the same for the samples DR-0 and DR-5, *i.e.*, decreasing with aging time. The retention rate of the tensile strength was further analyzed to distinguish the differences in hydrolysis between the DR-0 and the DR-5 samples, as shown in Fig. 6(b). Impressively, the retention rate of the DR-5 sample is higher than that of the DR-0 sample during the entire aging time span. After 5 days of aging, the retention rate of tensile strength of the DR-5 sample is 50% in comparison with only 30% of the DR-0 sample. It has to be explained that the initial increase in both tensile strength and retention rate, *e.g.*, after one day, is due to a cold crystallization under the aging conditions (Fig. S5 in ESI). These results confirm that the solid-state drawing could not only increase the mechanical performance of PGA but also could improve its resistance to hydrolysis.

Hydrolysis behavior has close relationship with the carboxyl index, intrinsic viscosity, melting point and crystallinity of the hydrolyzed samples. FTIR was used first to characterize the chemical structure changes of the DR-0 and DR-5 samples (Fig. S7 in ESI). Hydrolysis makes short(er) PGA chains, leading to an obvious increase in the content of terminal carboxyl groups and the deterioration of mechanical properties. Thus, carboxyl index (CI) calculated by the ratio of I_{3290} to I_{2960} is used to quantify the degree of polyester degradation,[34,35] where the I_{3290} is the absorption band intensity at 3290 cm^{-1} (corresponding to O—H stretching vibration of the —COOH group), and the I_{2960} is the internal standard band intensity at 2960 cm^{-1} (corresponding to C—H stretching vibration of the $—CH_2—$), as shown in Fig. 7(a). The CI of both samples increases during aging due to the intrinsic hydrolytic feature of PGA, but the CI of the DR-5 is much smaller than DR-0 notably at the last stage, *e.g.*, after 7 days the CI of DR-5 is 0.32 in comparison with 0.99 of DR-0. The intrinsic viscosity [η] of the PGA samples was applied to monitor the molecular weight change of PGA as a function of aging time, as shown in Fig. 7(b). The [η] of both samples decreases with time due to the hydrolysis of ester groups in humid conditions. However, the intrinsic viscosity of the DR-5 is much higher than that of the DR-0 at varied time. These results indicate that the intrinsic hydrolytic degradation of PGA in was slowed down by the solid-state drawing.

Generally, polymer with higher molecular weight possesses higher melting point (T_m) and lower X_c.[36] The changes of T_m and X_c of the PGA samples with aging time are shown in Figs. 7(c) and 7(d), while the corresponding DSC curves and thermal parameters are shown in Fig. S6, Tables S4 and S5 (in ESI). The T_m of the DR-0 sample drops from 224.4 °C to 216.7 °C after 7 days, but the T_m of the DR-5 sample remains almost constant until 3 days, and drops less than the DR-0 sample. In the meantime, the X_c of DR-0 and DR-5 gradually increases with aging time due to the lower molecular weight after hydrolysis and better crystallization ability of the short(er) chains. In addition, the plasticizing effect of water molecules may also contribute to the increase of X_c by reducing the T_g and improving the crystallization ability of the molecules.[34] After 7 days, the X_c of DR-0 increased by 17% in comparison with 8% of DR-5. The variation in thermal parameters also indicates a better resistance of PGA to hydrolysis after the solid-state drawing, and consisting with the above chemical structure analysis.

Mechanism of Resistance towards Hydrolysis Assisted by Solid-state Drawing

The mechanism of hydrolysis resistance from the perspective of structure evolution of the crystalline and amorphous regions during the solid-state drawing is schematically illustrated in Fig. 8. The crystalline region of PGA sample without drawing is isotropic, and the amorphous region is dominated by MAF with large(er) free volume (DR=0, Fig. 8a). The loose structure makes water molecules easier penetrate into the PGA matrix in a humid environment, leading to a faster hydrolysis starting from the amorphous region. Based on above discussion, the crystalline regions of fibrous PGA become oriented in the stretching direction at a mediate drawing ratio, such as DR=3–5, forming a periodically arranged fibrous crystals (Figs. 8b and 8c). The lateral size of lamellae increases first and then decreases with increasing the drawing ratio, while the average length of fibrous crystals increases monotonically. Meanwhile, more and more tightly arranged RAF with less free volume are formed accompanied by a consumption of MAF (Figs. 8b to 8c).

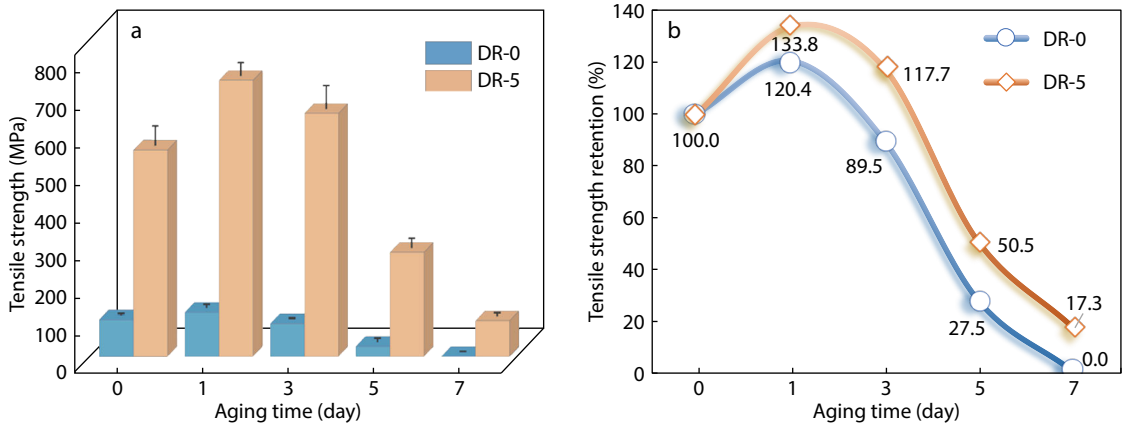

Fig. 6 (a) Tensile strength changes and (b) the corresponding tensile strength retention rate of DR-0 and DR-5 samples as a function of aging time.

https://doi.org/10.1007/s10118-022-2760-y

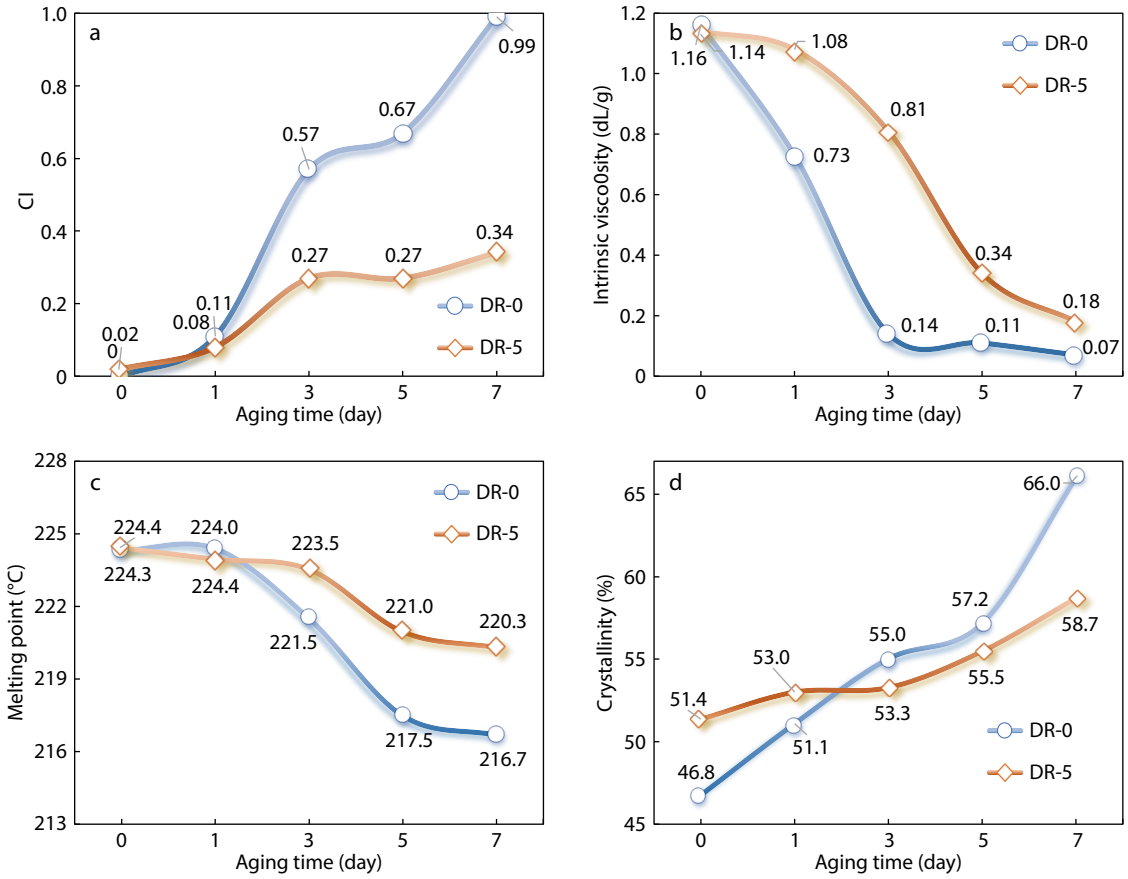

Fig. 7 (a) Carboxyl index (CI), (b) intrinsic viscosity, (c) melting point (T_m), and (d) crystallinity (X_c) of DR0 and DR5 after aged for different days. The T_m and X_c were obtained from the second DSC heating scans as shown in ESI.

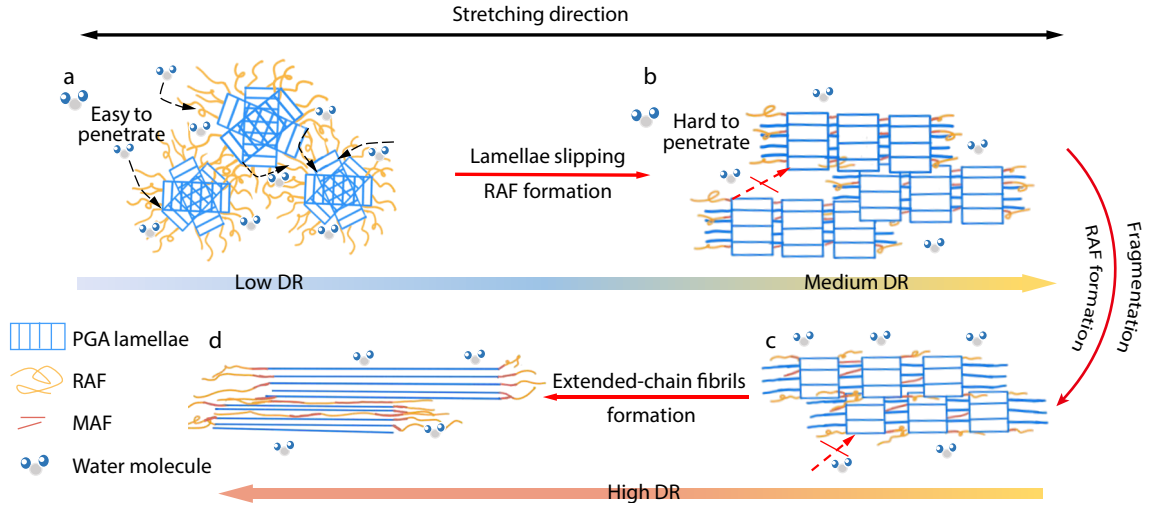

Fig. 8 Schematic diagram of structure evolution of fibrous PGA during solid-state drawing and the mechanism of resistance to hydrolysis assisted by solid-state drawing.

Compared with isotropic and loose crystal structures (DR-0), the PGA matrix with fibrous crystals in combination with large(r) X_{RAF} is more resistance to penetration of water molecules, thus better resistance to hydrolysis (Figs. 8b and 8c). At high drawing ratios such as DR=7, the crystalline region has been mainly dominated by extended-chain fibrils structures rather than chain-folded lamellae (Fig. 8d), and the highly oriented structures are responsible to its high tensile strength and modulus.

CONCLUSIONS

In this work, solid-state drawing was applied to make fibrous PGA with comprehensive properties such as superior tensile

https://doi.org/10.1007/s10118-022-2760-y

strength (~1 GPa), high toughness (elongation at break >20%) and resistance to hydrolysis. The solid-state drawing constructed oriented fibrous crystals and large(r) X_{RAF} in the amorphous region, which not only resulted in better mechanical performance but also could improve the resistance of PGA towards hydrolysis by hindering the penetration of water molecules. The transformation of structures of PGA from isotropic spherulites to fibrous crystals in the stretching direction and an obvious increase in tightly arranged RAF were well monitored by using SAXS and TMDSC. The relationships between the performance and the structures are well corelated. In addition, the heat capacity for totally mobile amorphous PGA (ΔC_p^0=0.64 J·g^{-1}·°C^{-1}) is the first time reported. Therefore, this work provides a facile method to improve both mechanical properties and resistance towards hydrolysis of PGA materials, which may expand the application range of PGA in commodity area.

NOTES

The authors declare no competing financial interest.

Electronic Supplementary Information

Electronic supplementary information (ESI) is available free of charge in the online version of this article at http://doi.org/10.1007/s10118-022-2760-y.

ACKNOWLEDGMENTS

This work was financially supported by the National Natural Science Foundation of China (Nos. 52073123 and 51873082), the Distinguished Young Natural Science Foundation of Jiangsu Province (No. BK20200027). The authors would also like to acknowledge Shanghai Pujing Chemical Industry Co., Ltd. for supplying the PGA raw materials.

REFERENCES

1 Yu, C.; Bao, J.; Xie, Q.; Shan, G. Crystallization behavior and crystalline structural changes of poly(glycolic acid) investigated *via* temperature-variable WAXD and FTIR analysis. *CrystEngComm* **2016**, *18*, 7894–7902.
2 Chatani, Y.; Suehiro, K.; Okita, Y.; Tadokoro, H. H. Structural studies of polyesters. I. Crystal structure of polyglycolide. *Macromol. Chem. Phys.* **1968**, *113*, 215–229.
3 Yamane, K.; Kawakami, Y. *Polyhydroxycarboxylic acid and its production process*, US, **2006**.
4 Shawe, S.; Buchanan, F.; Harkin-Jones, E.; Farrar, D. A study on the rate of degradation of the bioabsorbable polymer polyglycolic acid (PGA). *J. Mater. Sci.* **2006**, *41*, 4832–4838.
5 Stloukal, P.; Jandikova, G.; Koutny, M.; Sedlařík, V. Carbodiimide additive to control hydrolytic stability and biodegradability of PLA. *Polym. Test.* **2016**, *54* , 19–28.
6 Nishino, K.; Shindo, Y.; Takayama, T.; Ito, H. Improvement of impact strength and hydrolytic stability of PC/ABS blend using reactive polymer. *J. Appl. Polym. Sci.* **2017**, *134*, 1–6.
7 Rodriguez, E.; Shahbikian, S.; Marcos, B.; Huneault, M. A. Hydrolytic stability of polylactide and poly(methyl methacrylate) blends. *J. Appl. Polym. Sci.* **2018**, *135*, 1–14.
8 Špírková, M.; Hodan, J.; Kobera, L.; Kredatusová, J. The influence of the length of the degradable segment on the functional properties and hydrolytic stability of multi-component polyurethane elastomeric films. *Polym. Degrad. Stabil.* **2017**, *137*, 216–228.
9 Mazurek-Budzyńska, M.; Behl, M.; Razzaq, M. Y.; Nöchel, U. Hydrolytic stability of aliphatic poly(carbonate-urea-urethane)s: Influence of hydrocarbon chain length in soft segment. *Polym. Degrad. Stabil.* **2019**, *161*, 283–297.
10 Park, T. G. Degradation of poly(lactic-*co*-glycolic acid) microspheres: effect of copolymer composition. *Biomaterials* **1995**, *16*, 1123–1130.
11 Li, Y.; Yuan, L.; Ming, H.; Li, X. Enhanced hydrolytic resistance of fluorinated silicon-containing polyether urethanes. *Biomacromolecules* **2020**, *21*, 1460–1470.
12 Madden, D.G.; Albadarin, A.B.; O'Nolan, D.; Cronin, P. Metal-organic material polymer coatings for enhanced gas sorption performance and hydrolytic stability under humid conditions. *ACS Appl. Mater. Interfaces* **2020**, *12*, 33759–33764.
13 Xu, H.; Zhong, G. J.; Fu, Q.; Lei, J. Formation of shish-kebabs in injection-molded poly(*l*-lactic acid) by application of an intense flow field. *ACS Appl. Mater. Interfaces* **2012**, *4*, 6774–6784.
14 Zhou, S.-Y.; Niu, B.; Xie, X. L.; Ji, X. Interfacial shish-kebabs lengthened by coupling effect of in situ flexible nanofibrils and intense shear flow: achieving hierarchy to conquer the conflicts between strength and toughness of polylactide. *ACS Appl. Mater. Interfaces* **2017**, *9*, 10148–10159.
15 Zhang, Z. C.; Sang, Z. H.; Huang, Y. F.; Ru, J. F. Enhanced heat deflection resistance *via* shear flow-induced stereocomplex crystallization of polylactide systems. *ACS Sustain. Chem. Eng.* **2017**, *5*, 1692–1703.
16 Browning, A.; Chu, C. C. The effect of annealing treatments on the tensile properties and hydrolytic degradative properties of polyglycolic acid sutures. *J. Biomed. Mater. Res. Part A* **1986**, *20*, 613–632.
17 Sangroniz, A.; Chaos, A.; Iriarte, M.; del Río, J. Influence of the rigid amorphous fraction and crystallinity on polylactide transport properties. *Macromolecules* **2018**, *51*, 3923–3931.
18 Nassar, S. F.; Domenek, S.; Guinault, A.; Stoclet, G. Structural and dynamic heterogeneity in the amorphous phase of poly(L,L-lactide) confined at the nanoscale by the coextrusion process. *Macromolecules* **2018**, *51*, 128–136.
19 Montes de Oca, H.; Ward, I. M. Structure and mechanical properties of PGA crystals and fibres. *Polymer* **2006**, *47*, 7070–7077.
20 Montes de Oca, H.; Ward, I. M.; Klein, P. G.; Ries, M. E. Solid state nuclear magnetic resonance study of highly oriented poly(glycolic acid). *Polymer* **2004**, *45*, 7261–7272.
21 Delpouve, N.; Stoclet, G.; Saiter, A.; Dargent, E. Water barrier properties in biaxially drawn poly(lactic acid) films. *J. Phys. Chem. B* **2012**, *116*, 4615–4625.
22 Lee, S.; Hongo, C.; Nishino, T. Crystal modulus of poly(glycolic acid) and its temperature dependence. *Macromolecules* **2017**, *50*, 5074–5079.
23 An, M.; Xu, H.; Lv, Y.; Gu, Q. An *in situ* small-angle X-ray scattering study of the structural effects of temperature and draw ratio of the hot-drawing process on ultra-high molecular weight polyethylene fibers. *RSC Adv.* **2016**, *6*, 51125–51134.
24 Cao, T.; Chen, X.; Lin, Y.; Meng, L. Structural evolution of UHMWPE fibers during prestretching far and near melting temperature: an *in situ* synchrotron radiation small- and wide-angle X-ray scattering study. *Macromol. Mater. Eng.* **2018**, *303*, 1700493.
25 Chen, X.; Lv, F.; Su, F.; Ji, Y. Deformation mechanism of *i*PP under uniaxial stretching over a wide temperature range: an *in-situ*

synchrotron radiation SAXS/WAXS study. *Polymer* **2017**, *118*, 12–21.
26 Wang, Z.; Ma, Z.; Li, L. Flow-induced crystallization of polymers: molecular and thermodynamic considerations. *Macromolecules* **2016**, *49*, 1505–1517.
27 Ruland, W. Small-angle scattering studies on carbonized cellulose fibers. *J. Polym. Sci. Polym. Symp.* **2010**, *28*, 143–151.
28 Perret, R.; Ruland, W. Single and multiple X-ray small-angle scattering of carbon fibres. *J. Appl. Crystallogr* **1969**, *2*, 209–218.
29 Perret, R.; Ruland, W. The microstructure of PAN-base carbon fibres. *J. Appl. Crystallogr.* **1970**, *3*, 525–532.
30 Montes de Oca, H.; Farrar, D. F.; Ward, I. M. Degradation studies on highly oriented poly(glycolic acid) fibres with different lamellar structures. *Acta Biomaterialia* **2011**, *7*, 1535–1541.
31 Czerniecka-Kubicka, A.; Janowski, G.; Pyda, M.; Frącz, W. Biocomposites based on the poly(3-hydroxybutyrate-*co*-3-hydroxyvalerate) matrix with the hemp fibers: thermal and mechanical properties. *J. Therm. Anal. Calorimetry* **2021**, *147*, 1017–1029.
32 Cao, Y.; Xu, P.; Yang, W.; Zhu, X. UV resistant PBT nanocomposites by reactive compatibilization and selective distribution of tailor-made double-shelled TiO_2 nanohybrids. *Compos. Part B: Eng.* **2021**, *205*, 108510.
33 Fechine, G. J. M.; Rabello, M. S.; Souto Maior, R. M.; Catalani, L. H. Surface characterization of photodegraded poly(ethylene terephthalate). The effect of ultraviolet absorbers. *Polymer* **2004**, *45*, 2303–2308.
34 King, E.; Robinson, S.; Cameron, R. E. Effect of hydrolytic degradation on the microstructure of quenched, amorphous poly(glycolic acid): an X-ray scattering study of hydrated samples. *International* **1999**, *48*, 915–920.
35 Woodard, L. N.; Grunlan, M. A. Hydrolytic degradation and erosion of polyester biomaterials. *ACS Macro Lett.* **2018**, *7*, 976–982.
36 Organ, S. J. Variation in melting point with molecular weight for hydroxybutyrate/hydroxyvalerate copolymers. *Polymer* **1993**, *34*, 2175–2179.

https://doi.org/10.1007/s10118-022-2760-y